Inorganica Chimica Acta, 143 (1988) 59–70

Cyclopentadienyl Iron Xanthate Complexes. Crystal and Molecular Structure and Electrochemical Reduction of η-$C_5R_5Fe(CO)_2(\eta^1$-SC(S)OEt) (R = H or CH_3)

MOISÉS MORÁN, ISABEL CUADRADO, JOSÉ R. MASAGUER

Departamento de Química. C-VIII, Universidad Autónoma de Madrid, Cantoblanco, 28049-Madrid, Spain

JOSÉ LOSADA

Departamento de Química Inorgánica y Analítica, E.T.S. de Ingenieros Industriales, Universidad Politécnica de Madrid, 28001-Madrid, Spain

CONCEPCION FOCES-FOCES and FELIX H. CANO

Departamento de Rayos X, Instituto Rocasolano, C.S.I.C., Serrano 119, 28006-Madrid, Spain

(Received May 20, 1987)

Abstract

Complexes η-$C_5R_5Fe(CO)_2(\eta^1$-SC(S)OEt) (R = H, (**1**) and R = CH_3 (**2**)) have been analysed by X-ray diffraction techniques. **1**: $P2_12_12_1$ 11.3560(5), 10.8595(4), 10.1158(3) Å, Z = 4; 1023 observed reflexions, R and R_w 0.069 and 0.073. **2**: *Pbca*, 15.6907(11), 15.4566(13), 14.3083(11) Å, Z = 8; 2271 observed reflexions, R and R_w being 0.071, 0.073. The coordination is quite similar for both compounds with the xanthate monodentate ligand almost perpendicular to the ring planes and a relative twist, one from each other of about 10°. The reductive electrochemistry of both complexes has been examined by cyclic voltammetry and coulometry. In a carbon electrode the first-one electron reduction step can be ascribed to the formation of corresponding carbonyl dimers. In a mercury electrode, the first reduction step of **1** leads to a bond rupture process with formation of a mercury compound $[CpFe(CO)_2]_2Hg$ and further reduction to the anion $CpFe(CO)_2^-$. However, the behaviour of the pentamethylcyclopentadienyl complex (**2**) is quite different, and it is reduced in a three step process.

Introduction

The chemistry and structural aspects of the xanthate complexes have been extensively studied [1–4]. However, organometallic complexes of xanthates are less numerous [5–7] and only a very few complexes are known in which the mode of coordination of this ligand is monodentate [8].

Iron cyclopentadienyl compounds of this type, η-$C_5H_5Fe(CO)_2X$ (X = monodentate ligand) have been employed as catalytic agents in hydroformylation reaction of olefins and in the polymerization of α-olefins by means of Ziegler-Natta catalysts. The catalytic activity depends on the substituent in the cyclopentadienyl ring [9, 10].

In other cases, it has been found that the rate of substitution of the carbonyl groups in compounds similar to those indicated, is drastically modified by the presence of methyl groups in the cyclopentadienyl ring [11].

However, there are very few systematic studies which compare the structures and properties of the peralkyl-substituted and non-substituted cyclopentadienyl complexes [12].

In a previous study [13], we reported the synthesis, characterization and reactivity of the monodentate xanthate complexes η-$C_5R_5Fe(CO)_2(\eta^1$-SC(S)OEt) (R = H or Me). In this work we report the comparison between the crystal structures of η-$C_5H_5Fe(CO)_2(\eta^1$-SC(S)OEt) (**1**) and its pentamethylcyclopentadienyl analogue η-$C_5Me_5Fe(CO)_2(\eta^1$-SC(S)OEt) (**2**) in order to analyse the influence of the electronic factors on the structure and reactivity of these compounds. Moreover, the integrated intensities data, force constants and dipole moment derivatives for the carbonyl stretching vibrations in the IR spectra are analysed. The relative magnitudes of some parameters in these compounds, allow us to understand the nature of their metal–ligand bonds. Integrated intensity measurements of the ν(CO) vibrations in transition metal carbonyl complexes have given additional information on the electronic character of the CO group. In addition, the electrochemical reduction in THF, at carbon and mercury electrodes has been examined by cyclic voltammetry.

Experimental

The compounds η-$C_5H_5Fe(CO)_2(\eta^1$-SC(S)OEt) (**1**) and η-$C_5Me_5Fe(CO)_2(\eta^1$-SC(S)OEt) (**2**) were pre-

0020-1693/88/$3.50

pared by reaction between the dimers $[\eta\text{-}C_5R_5Fe(CO)_2]_2$ (R = H or Me) and the dixanthogen, $[SC(S)OEt]_2$, according to the method described previously [13]. The compounds were purified by recrystallization from cyclohexane, and characterized by IR and ^1H and ^{13}C NMR spectra.

The IR spectra were recorded on a Nicolet 5DX-FT-IR spectrophotometer. The solid spectra were taken using Nujol mulls between CsI windows. The solution spectra were recorded in CS_2 solution using 1.0 and 0.1 mm matched NaCl cells. Sample concentrations were in the range 10^{-3}–10^{-4} M.

Spectra for intensity measurements were recorded in absorbance. The areas of the bands were determined using the software of the spectrophotometer. The integrated intensities were determined at a number of concentrations and extrapolated to zero concentration [14]. Data were analysed by the linear least-squares method.

Experimental X-ray Crystallography

The main characteristics of the analysis are given in Table I. It should be noted that in spite of the Cu radiation used the possible fluorescent radiation was no trouble at any stage of the analysis. The structure of the permethylated complex **2**, was solved from **1** by means of orientation and translation function of the Patterson map [15]. The hydrogen atoms in **2** have to be kept fixed in the final stages of the refinement. Final atomic coordinates are given in Tables II and III.

TABLE I. Crystal Analysis Parameters at Room Temperature

	1	**2**
Crystal data		
Formula	$C_{10}H_{10}O_3S_2Fe$	$C_{15}H_{25}O_3S_2Fe$
Crystal habit	red, square prism	red, pseudospherical polyhedron
Crystal size (mm)	0.20 × 0.17 × 0.17	0.43–0.60
Symmetry	orthorhombic, $P2_12_12_1$	orthorhombic, *Pbca*
Unit cell determination	least-squares fit from 86 reflexions ($\theta < 45°$)	least-squares fit from 89 reflexions ($\theta < 45°$)
Unit cell dimensions	11.3560(5), 10.8595(4), 10.1158(3) Å	15.6907(11), 15.4566(13), 14.3083(11) Å
Packing: V (Å^3), Z	1247.5(1), 4	3470.1(5), 8
D_c (g cm^{-3}), M, $F(000)$	1.588, 298.2, 608	1.415, 368.3, 1536
μ (cm^{-1})	127.65	92.77
Experimental data		
Technique	four circle diffractometer: Philips PW1100 bisecting geometry graphite oriented monochromator: Cu Kα $\omega/2\theta$ scans, scan width: 1.5° detector apertures 1° × 1°, up θmax. 65° 1 min/reflex.	four circle diffractometer: Philips PW1100 bisecting geometry graphite oriented monochromator: Cu Kα $\omega/2\theta$ scans, scan width: 1.5° detector apertures 1° × 1°, up θmax. 65° 1 min/reflex.
No. reflexions		
Independent	1229	2930
Observed	1023 ($3\sigma(I)$ criterion)	2271 ($3\sigma(I)$ criterion)
Standard reflexions	2 reflexions every 90 min variation: no	2 reflexions every 90 min variation: no
Max–min transmission factors	0.827–1.217	0.490–1.214
Solution and refinement		
Solution	Patterson and Fourier maps	Patterson and Fourier maps
Refinement	L.S. on Fobs with 1 block	L.S. on Fobs with 1 block
Parameters		
Number of variables	145	190
Degrees of freedom	878	2081
Ratio of freedom	7.1	12.0
H atoms	difference synthesis	difference synthesis
Final shift/error	0.28	0.18
w-scheme	empirical as to give no trends in $\langle w\Delta^2F\rangle$ *vs.* $\langle F_o\rangle$ or $\langle \sin\theta/\lambda\rangle$	empirical as to give no trends in $\langle w\Delta^2F\rangle$ *vs.* $\langle F_o\rangle$ or $\langle \sin\theta/\lambda\rangle$
Max. thermal value	$U22$(C14) = 0.22(3) Å^2	$U22$(C17) = 0.15(1) Å^2
Final ΔF peaks	0.66 e Å^{-3}	0.71 e Å^{-3}
Final R and R_w	0.069, 0.073	0.071, 0.073
Computer and programs	VAX 11/750, Dirdif [15], Difabs [16], XRAY76 [17]	VAX 11/750, Dirdif [15], Difabs [16], XRAY76 [17]
Scattering factors	Int. Tables for X-ray Crystallography [18]	Int. Tables for X-ray Crystallography [18]

TABLE II. Final Atomic Coordinates and Thermal Parameters for **1**[a]

Atom	*x/a*	*y/b*	*z/c*	$U_{eq} \times 10^4$
Fe	0.1829(2)	0.2800(2)	0.7758(2)	367(5)
S1	0.0533(3)	0.4062(3)	0.8806(4)	430(10)
S2	−0.0366(3)	0.4653(4)	1.1460(4)	557(13)
C3	0.0560(9)	0.3898(10)	1.0501(12)	290(33)
O4	0.1400(8)	0.3140(8)	1.0925(9)	434(29)
C5	0.1521(12)	0.2872(17)	1.2313(14)	599(50)
C6	0.2644(17)	0.2175(23)	1.2491(17)	963(82)
C7	0.3003(11)	0.3280(13)	0.8756(12)	407(40)
O8	0.3791(8)	0.3607(10)	0.9380(11)	569(35)
C9	0.1492(12)	0.1508(13)	0.8766(12)	401(41)
O10	0.1299(10)	0.0637(10)	0.9343(12)	621(38)
C11	0.0990(15)	0.2177(20)	0.6017(16)	644(58)
C12	0.1080(18)	0.3446(19)	0.5992(19)	724(73)
C13	0.2226(21)	0.3759(19)	0.5992(20)	773(76)
C14	0.2873(15)	0.2761(36)	0.6112(17)	990(103)
C15	0.2107(29)	0.1721(19)	0.6155(17)	936(99)

[a] $U_{eq} = (1/3)\Sigma(U_{ij}a^*_i a^*_j a_i a_j \cos(a_i, a_j))$.

Electrochemical Measurement

The cyclic voltammetric experiments were carried out by the use of a Metrohm VA-Scanner, in conjunction with a Metrohm VA-detector and a Linseis LY-17100 X-Y recorder. Fast scan cyclic voltammograms were recorded on a Hitachi VC-6015 digital storage oscilloscope. The coulometric experiments were carried out with a Beckman Electroscan 30 instrument. The electrochemical measurements were performed in a three-electrode cell, with a carbon glassy working electrode, or an hanging mercury drop electrode (HMDE), a platinum wire auxiliary electrode and an aqueous saturated calomel-electrode (SCE). The reference electrode was separated from the test solution by a Vycor frit and a bridge of $[NBu^n_4][PF_6]$ (0.1 M) in THF.

A sample solution contained a metal complex (10^{-3}–10^{-4} M) and a supporting electrolyte, $[NBu^n_4][PF_6]$ (0.1 M) [19]. Tetrahydrofuran (THF), was purified using the 'ketyl method'.

In the coulometry, the working electrode was a platinum mesh or a mercury pool electrode.

Results and Discussion

Description of the Molecular Structure

The metal atom presents in both complexes the same pseudooctahedral coordination (Fig. 1), with no significative differences in the amount of the distortions in the angles at Fe (Table IV) *versus* the theoretical ones (125.3, 90.0°). These angular values indicate that the sulphur and the carbonyl carbon atoms are distorted towards the ring. The relative position of the rings and the ligands can be described by the pseudotorsion angles around ClOO....Fe (see Table V and Fig. 2, ClOO being the centroid of the five-membered ring). There is a relative twist of −9.6(1)° between that relative position in the two complexes. It is also apparent that the dihedral apertures between carbonyls are greater

TABLE III. Final Atomic Coordinates and Thermal Parameters for **2**[a]

Atom	*x/a*	*y/b*	*z/c*	$U_{eq} \times 10^4$
Fe	0.21194(5)	0.05956(5)	0.11567(6)	111(2)
S1	0.10455(9)	0.15093(9)	0.15905(9)	152(4)
S2	−0.02283(11)	0.26685(12)	0.07521(13)	337(5)
C3	0.05165(33)	0.19291(33)	0.06424(39)	128(15)
O4	0.07877(25)	0.16155(28)	−0.01746(26)	195(12)
C5	0.03931(45)	0.19119(48)	−0.10393(45)	320(20)
C6	0.07914(66)	0.13808(75)	−0.17999(50)	585(33)
C7	0.14366(40)	0.00169(39)	0.04031(46)	218(17)
O8	0.10227(40)	−0.03946(36)	−0.00743(46)	506(19)
C9	0.24851(37)	0.13166(39)	0.02731(41)	171(16)
O10	0.27489(30)	0.17683(38)	−0.02709(38)	411(17)
C11	0.32170(42)	0.07525(42)	0.20054(48)	274(19)
C12	0.25073(54)	0.05945(54)	0.25756(42)	361(22)
C13	0.21464(42)	−0.02185(50)	0.23124(50)	340(21)
C14	0.26670(43)	−0.05652(42)	0.16027(51)	288(19)
C15	0.33137(38)	0.00349(43)	0.13986(44)	251(19)
C16	0.38148(63)	0.15114(69)	0.20498(90)	715(37)
C17	0.22117(86)	0.11635(102)	0.33705(61)	944(53)
C18	0.13898(62)	−0.06730(103)	0.27636(92)	913(51)
C19	0.25951(81)	−0.14512(49)	0.11494(83)	660(35)
C20	0.40346(57)	−0.00820(78)	0.07207(67)	600(33)

[a] $U_{eq} = (1/3)\Sigma(U_{ij}a^*_i a^*_j a_i a_j \cos(a_i, a_j))$.

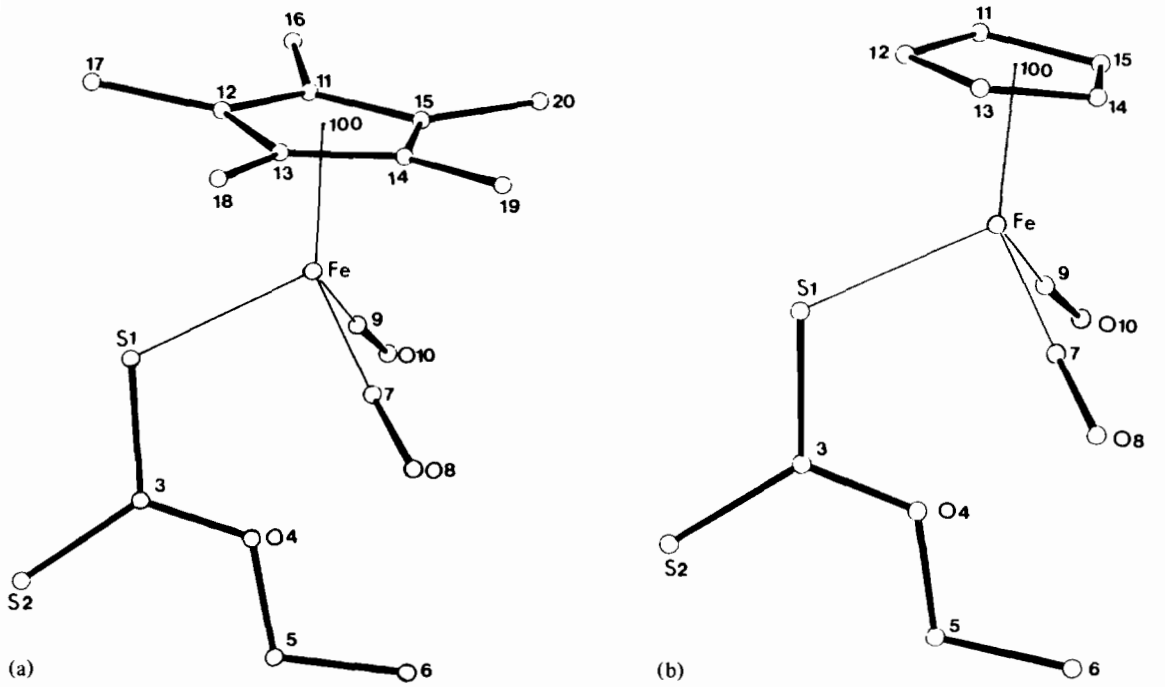

Fig. 1. ORTP [20] drawing with atom labeling of (a) complex **1**, (b) complex **2**.

TABLE IV. Selected Bond Distances (Å) and Angles (°)

	1	2		1	2
Fe–S1	2.274(4)	2.285(2)	Fe–C7	1.752(13)	1.764(6)
Fe–C9	1.775(13)	1.780(6)	F3–C11	2.114(17)	2.121(7)
Fe–C12	2.099(19)	2.120(6)	Fe–C13	2.117(21)	2.078(7)
Fe–C14	2.045(17)	2.089(7)	Fe–C15	2.026(19)	2.094(6)
Fe–C100[a]	1.725(8)	1.723(8)	S1–C3	1.725(12)	1.718(6)
S2–C3	1.650(12)	1.642(5)	C3–O4	1.331(14)	1.335(7)
C5–O4	1.441(17)	1.457(8)	C5–C6	1.494(26)	1.500(12)
C7–O8	1.151(16)	1.137(9)	C9–O10	1.134(17)	1.125(8)
C11–C12	1.382(30)	1.402(10)	C11–C15	1.369(36)	1.417(9)
C12–C13	1.345(31)	1.429(11)	C13–C14	1.315(40)	1.409(10)
C14–C15	1.427(41)	1.405(9)			
C9–Fe–C100	124.4(6)	124.1(3)	C7–Fe–C100	124.6(5)	124.1(3)
C7–Fe–C9	93.9(6)	94.5(3)	S1–Fe–C100	119.2(4)	121.0(3)
S1–Fe–C9	94.0(4)	92.5(2)	S1–Fe–C7	92.6(4)	91.8(2)
Fe–S1–C3	112.9(4)	112.1(2)	S1–C3–S2	121.5(7)	122.1(3)
S2–C3–O4	125.1(9)	124.3(4)	S1–C3–O4	125.1(9)	124.3(4)
C3–O4–C5	120.5(10)	119.6(5)	O4–C5–C6	107.6(12)	105.5(6)
Fe–C7–O8	178.1(12)	176.3(6)	Fe–C9–O10	175.6(12)	177.2(5)
C12–C11–C15	107.1(20)	107.8(6)	C11–C12–C13	108.9(18)	108.3(6)
C12–C13–C14	109.4(23)	107.1(6)	C13–C14–C15	108.3(21)	108.5(6)
C11–C15–C14	106.0(24)	108.2(6)			

Separation from the five-membered ring

1	Fe	1.722(2)				
2	Fe	1.723(1)	C(16)	0.064(12)	C17	0.118(12)
	C18	0.044(13)	C(19)	0.119(11)	C20	0.076(10)

[a]C100 means the centroid of the five-membered ring.

TABLE V. Selected Torsion Angles (°)

	1	2
C100–Fe–S1–C3	176.0(6)	177.7(4)
Fe–S1–C3–S2	−175.9(6)	−174.6(3)
S1–C3–O4–C5	−178.1(9)	179.8(4)
C11–C12–C13–C14	−4.6(26)	2.3(8)
C13–C14–C15–C11	1.5(28)	1.9(8)
C15–C11–C12–C13	5.5(24)	−1.2(8)
C11–C100–Fe–C7	167.2(12)	159.2(5)
C11–C100–Fe–C9	42.3(14)	34.2(6)
C11–C100–Fe–S1	−76.3(12)	−83.9(5)
C13–C100–Fe–C7	−48.1(15)	−56.6(6)
C13–C100–Fe–C9	−173.0(13)	178.3(5)
C13–C100–Fe–S1	68.5(13)	60.3(6)
C15–C100–Fe–C7	96.4(17)	86.9(6)
C15–C100–Fe–S1	−147.0(16)	−156.2(4)
Fe–S1–C3–O4	5.4(10)	3.6(5)
S2–C3–O4–C5	3.3(16)	−2.1(7)
C3–O4–C5–C6	−170.9(12)	−175.3(6)
C12–C13–C14–C15	1.9(28)	−2.6(8)
C14–C15–C11–C12	−4.2(25)	−0.5(8)
C12–C100–Fe–C7	−119.8(13)	−129.4(6)
C12–C100–Fe–C9	115.3(13)	105.5(6)
C12–C100–Fe–S1	−3.2(13)	−12.5(7)
C14–C100–Fe–C7	21.2(22)	15.1(7)
C14–C100–Fe–C9	−103.8(21)	−110.0(5)
C14–C100–Fe–S1	137.7(20)	132.0(4)
C15–C100–Fe–C9	−28.5(18)	−38.1(7)

(~125(1)°) than between these ligands and the sulphur atom S1 (~118(1)°).

The geometry of the Fe(CO) and FeS groups is within the reported values [21–23], the anticorrelation between Fe–C and Fe–S distances not being significant within precision. Moreover, no enlarging of the angle between ligands at the metal is noticeable in the permethylated complex [24].

The distances from the metal to the ring planes and to the centroid of them are equal (1.725(8) *versus* 1.723(8) and 1.722(2) *versus* 1.723(1) Å), so the Fe–C100 line is quite normal to the best plane through the rings. However the Fe–C(ring) distances are different in both cases (see Table IV). In complex **1** there are two short values [22] to C14 and C15, just corresponding to the longest C–C distance in the ring, *trans* to S1. In complex **2** the distribution is more even, with the longest C–C bond *cis* to S1. The C–C in the rings contraction [25, 26] is quite noticeable for the unmethylated case. The methyl groups are between 0.04(1) and 0.12(1) Å out of the least-squares plane through the ring and away from the metal [25, 26], C17 and C19, the nearest to S1 being the most deviated. The slight puckering of the rings is different: in complex **1** the conformation has a quasitwofold axis through C11–C12 while in **2** there is an approximate mirror

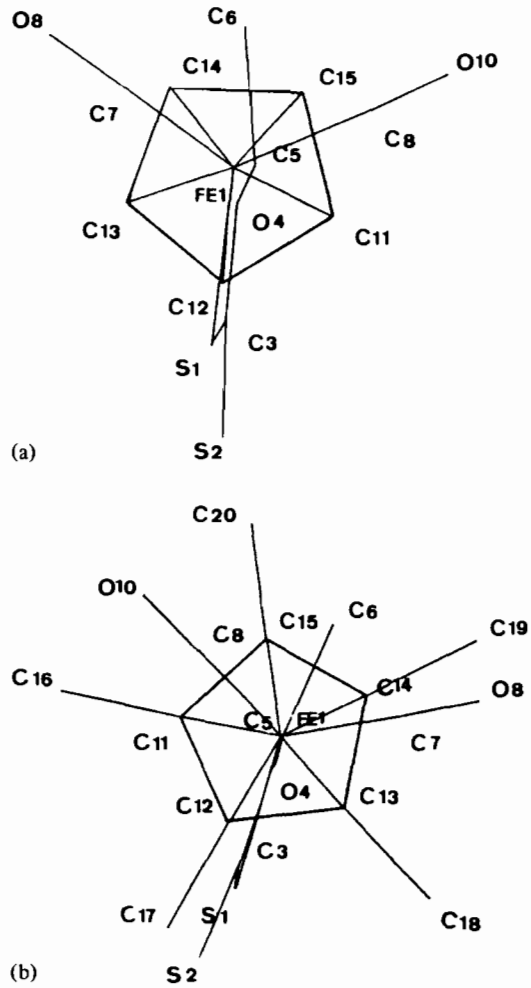

Fig. 2. A view of the structure of the complexes projected onto the ring planes: (a) η-$C_5H_5Fe(CO)_2(\eta^1$-SC(S)OEt (**1**), (b) η-$C_5Me_5Fe(CO)_2(\eta^1$-SC(S)OEt) (**2**).

plane through C13. The torsion angles at Fe–S1, S1–C3, C3–O4 and O4–C5 situate the xanthate ligand almost perpendicular to the ring plane. It is noteworthy that the Fe–carbonyl distances are not significantly different although the pentamethylcyclopentadienyl ligand is a more electron-donating ligand than cyclopentadienyl and also despite the fact that differences are observed in the carbonyl stretching vibrations (see below). Similar bond distances are observed for other monopentamethylcyclopentadienyl metal complexes [24, 27]. Significant shortening of metal–carbonyl bond lengths has been observed when two pentamethylcyclopentadienyl ligands are present [28].

We may describe the packing in terms of the Fe–C100 vectors. Complex **1** presents a noncentrosymmetrical packing with the complexes arranged in two sheets, with almost parallel Fe–C100 vectors, and antiparallel ones between sheets, both along the *c* axis. In **2** the arrangement is centrosym-

TABLE VI. Observed Frequencies, Calculated Force Constants, Infrared Intensities and Associated Dipole Moment Derivatives for the CO Stretching Modes of the Compounds $Cp^*Fe(CO)_2(\eta^1\text{-}SC(S)OEt)$ ($Cp^* = \eta\text{-}C_5H_5$ or $\eta\text{-}C_5Me_5$)

Complex	Nujol	CS_2	Vib. sym.	Force constants[a] (mdyn. $Å^{-1}$)	Absolute intensity[b] I (10^{-4} M^{-1} cm^{-2})	Dipole moment derivatives[c] μ'(FeCO)	$\frac{\mu'\text{FeCo A}'}{\mu'\text{FeCO A}''}$
$\eta\text{-}C_5H_5Fe(CO)_2(\eta^1\text{-}SC(S)OEt)$ (1)	2041.1vs, 2038.3sh, 2033vs	2039.3vs	A′	16.44 (K)	7.16	7.26	0.904
	2005.2vs, 1988.3vs, 1960.7sh	1996.4vs	A″	0.35 (K_i)	10.05	8.03	
$\eta\text{-}C_5Me_5Fe(CO)_2(\eta^1\text{-}SC(S)OEt)$ (2)	2016.4vs	2018.5vs	A′	16.09 (K)	8.90	7.86	0.850
	1975.8vs, 1966.6vs, 1938.2sh	1975.3vs	A″	0.34 (K_i)	13.45	9.24	

[a]K and K_i are the stretching and interaction force constants for the CO groups respectively. Values in CS_2 solution. [b]Average standard deviation ± 0.16. Values in CS_2 solution. Defined as $(2.303/Cl)\int$ band $\log(I_o/I)\,d\nu$, where C is the concentration in moles per liter and l is the cell pathlength in cm^{-1}. [c]Calculated from the equations $I_1(A') = 2G_{CO}\cos^2\alpha[\mu'(FeCO)(A')]^2$ and $I_2(A'') = 2G_{CO}\sin^2\alpha[\mu'(FeCO)(A'')]^2$ where $G_{CO} = 0.14585$, and α is the angle between the FeCO groups divided by two. From the crystal structure data $\alpha = 46.97°$ for **1** and $\alpha = 42.29°$ for **2**.

Fig. 3. The packing of the complexes: (a) $\eta\text{-}C_5H_5Fe(CO)_2(\eta^1\text{-}SC(S)OEt)$ (**1**), (b) $\eta\text{-}C_5Me_5Fe(CO)_2(\eta^1\text{-}SC(S)OEt)$ (**2**).

metric with antiparallel sheets of antiparallel molecules along approximately $(1\bar{1}1)$ plus another set of sheets quasinormal to the previous one (Fig. 3).

The observed frequencies (either in solid or in CS_2 solution), force constants and absolute intensities of the IR carbonyl stretching vibrations for the two complexes are given in Table VI.

The assignments of the ν(CO) vibrations are based on a local 'C_s' symmetry, for which there are two IR active stretching modes A′ and A″. The stretching, K, and interaction, K_i, force constants for the CO groups, expected for this symmetry have been calculated by the Cotton–Kraihanzel method [29]. The calculated values are very similar to those found in other iron dicarbonylcyclopentadienyl complexes $\eta\text{-}C_5R_5Fe(CO)_2X$ (X = halide, CN, SR, $SnCl_3$, $SP(S)(OR)_2$; R = H or Me) [30–33].

In solid state and in agreement with the different molecular packing for both complexes previously indicated, the IR spectra are quite different in the ν(CO) region. The non-centrosymmetric complex **1** presents, as expected, a higher number of bands due to ν(CO). However, in CS_2 solution only two ν(CO) bands are observed corresponding to the A′ and A″ modes (Fig. 4).

From the measure of the IR intensities I_1(A′) and I_2(A″), the characteristic MCO group dipole moment derivative for each of the A′ and A″ symmetry vibrations may be calculated and the results

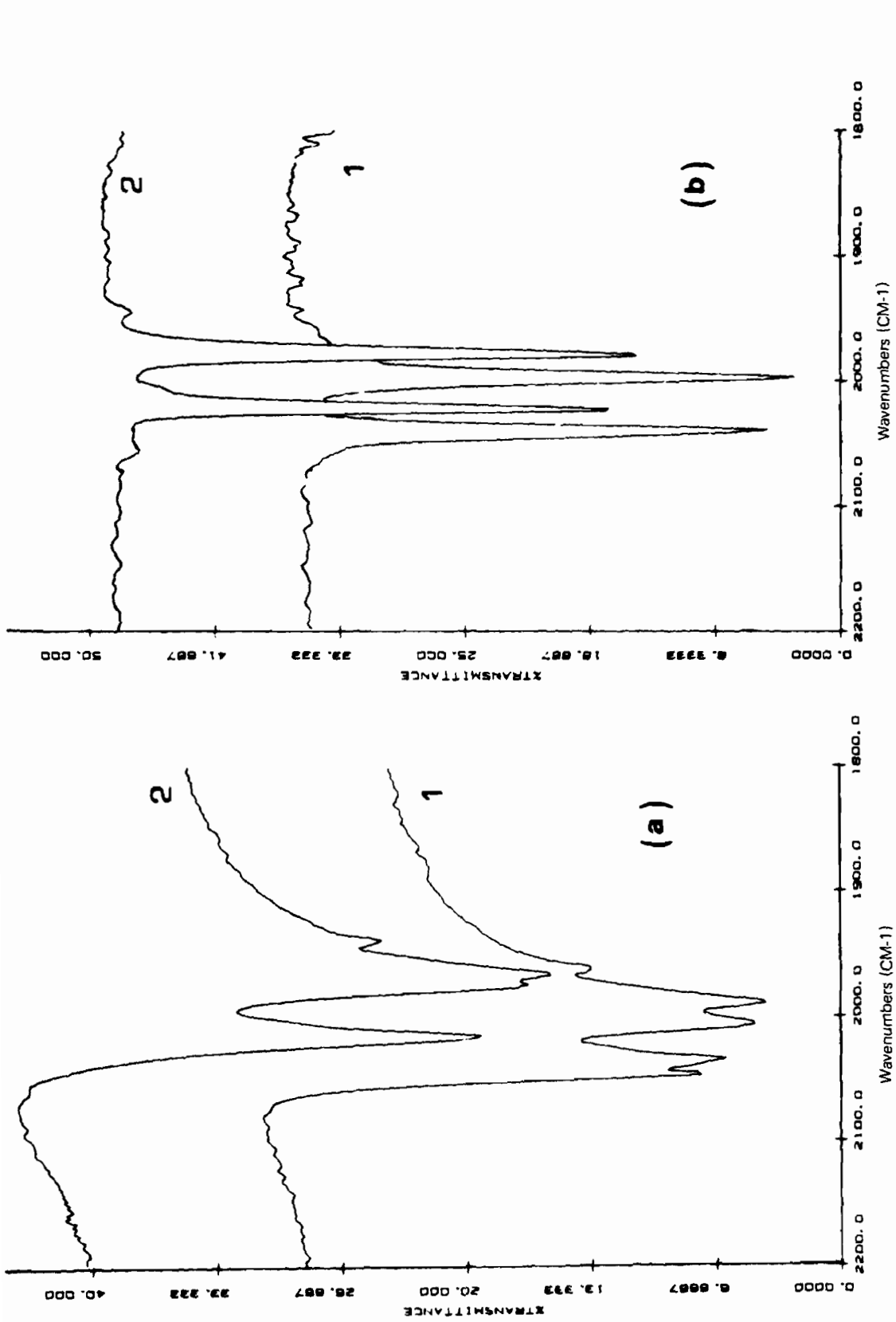

Fig. 4. IR spectra in the carbonyl region: (a) solid complexes η-$C_5H_5Fe(CO)_2(\eta^1$-SC(S)OEt) (1) and η-$C_5Me_5Fe(CO)_2(\eta^1$-SC(S)OEt) (2), (b) compounds 1 and 2 in CS_2 solution.

for the μ'(FeCO) are given in Table VI. From μ'(FeCO) values analysis for the two complexes it is possible to determine the influence of the cyclopentadienyl or pentamethylcylcopentadienyl ring on the electronic character of the bonded carbonyl group.

It can be seen, from the results shown in Table VI that the intensity and dipole moment derivative changes μ'(FeCO), are not uniformly distributed between the symmetric (A') and asymmetric (A'')-ν(CO) modes. This effect was explained for $M(CO)_5L$ species using a molecular orbital model to calculate the IR intensities and dipole moment derivatives [34], and similar arguments have been used for η-$C_5H_5Fe(CO)_2X$ compounds [30]. There is a net demand for π-electronic charge by the CO groups from the metal in the A' mode which is not present in the A'' mode [35]. This demand increases as the CO bond stretches, due to the π^* orbitals of the CO groups decreasing in energy. Since the intensity is largely dependent on the π-electronic charge in the MCO grouping, the expected order of dipole moment derivatives for η-$C_5H_5Fe(CO)_2X$ compounds is $\mu'(FeCO)(A') \geqslant \mu'(FeCO)(A'')$ [35, 36].

From the greater value of μ'(FeCO)(A'') over μ'(FeCO)(A') for both complexes **1** and **2** (Table VI), it is possible to conclude that there is not a sizable vibronic contribution from the cyclopentadienyl or pentamethylcyclopentadienyl ligand. Since the vibronic contributions are related to the extent of the back-bonding in the metal–ligand bond, this lead to the conclusion that there is little back-bonding contribution in the metal–cyclopentadienyl (or pentamethylcyclopentadienyl) moiety. Similar results have been obtained for the compounds η-$C_5H_5Fe(CO)_2X$ (X = Cl, I, CN, $SnCl_3$, $C(O)CH_3$) [30]. Furthermore, this conclusion is in agreement with the photo-electron spectroscopy measurements on several cyclopentadienylmetal complexes, which have indicated the ring carbon of the cyclopentadienyl residues to be slightly positively charged [37].

The intensities results given in Table VI indicate that the extent of Fe–CO bonding is greater in complex **2** than in complex **1**, which agrees with the higher electron-donating capacity of the pentamethylcyclopentadienyl ligand.

Electrochemical Studies

The cyclic voltammograms of all compounds at a carbon glassy electrode in THF solutions show two cathodic peaks (A, B) and an anodic peak (B'). In the case of η-$C_5H_5Fe(CO)_2(\eta^1$-SC(S)OEt) (**1**) at slow sweep rates (<100 mV s^{-1}) other anodic peak, B'_1, can be observed at more negative potentials (Fig. 5). In the CV curves of η-$C_5Me_5Fe(CO)_2(\eta^1$-SC(S)OEt), at scan rates <500 mV s^{-1}, the peak B' is completely absent in the first run being detected B'_1. However multicyclic voltammograms show that

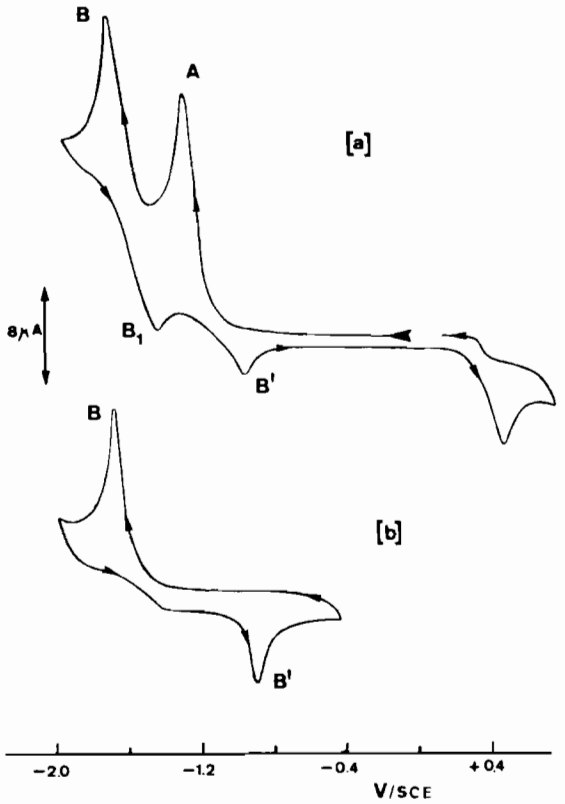

Fig. 5. Cyclic voltammograms in THF containing 0.1 M Bu_4NPF_6, at a C glassy electrode, scan rate 50 mV s^{-1} for: (a) η-$C_5H_5Fe(CO)_2(\eta^1$-SC(S)OEt) (**1**); (b) $[\eta$-$C_5H_5Fe(CO)_2]_2$.

on going through repeated cycles peak B'_1 disappears and the appearance of B' and decrease of A are observed (Fig. 6). If the scan is reversed after peak A, no anodic peak is observed for sweep rates from 10 mV s^{-1} to 1 V s^{-1} except one about +0.5 V which is attributable to oxidation of the release xanthate ligand.

The electrochemical irreversibility of the processes corresponding to peaks A and B is confirmed by the magnitude of the slopes in the plots of *Ep versus* log ν (ν, scan rate) [38], which are significantly larger than those expected for reversible processes.

The electrochemical reduction is diffusion controlled being the anodic current function ($^ip_c/\nu^{1/2}$) independent of scan rate (ν) over the range 0.1–1 V s^{-1}.

Complete electrolysis on a platinum electrode of all compounds, carried out at potentials 100 mV more negative than *Ep* of the peaks A and B (Table VII), requires 1 and 2 Faraday/mol respectively.

When the complexes were electrochemically reduced in a cell in the cavity of an EPR spectrometer at the potentials indicated above, after *Ep* of A and B, no species giving EPR signals were present.

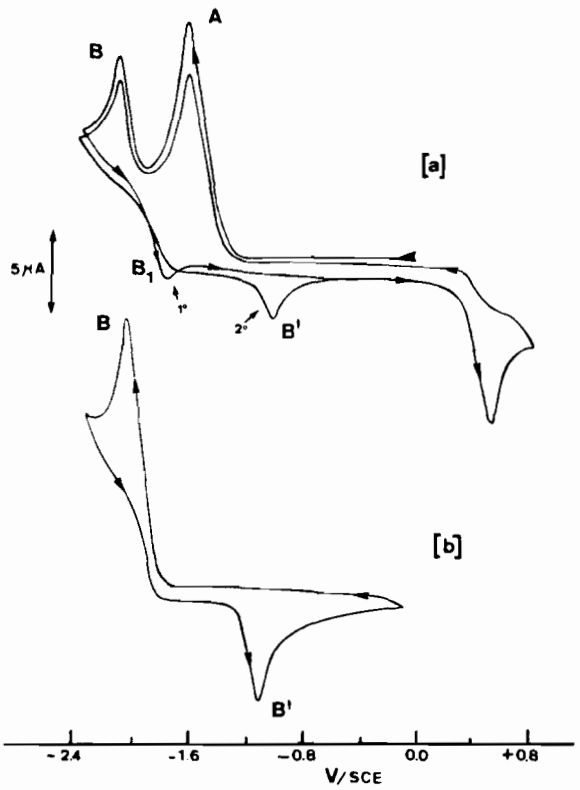

Fig. 6. (a) Multicyclic voltammogram for η-$C_5Me_5Fe(CO)_2$-(η^1-SC(S)OEt) (**2**) in THF containing 0.1 M Bu_4NPF_6, at a C glassy electrode; scan rate 0.2 V s^{-1}. (b) Cyclic voltammogram of $[\eta$-$C_5Me_5Fe(CO)_2]_2$ in the same conditions as (a).

The first peak A of the cyclic voltammograms can be ascribed to the formation of the corresponding dimer:

$$Cp^*Fe(CO)_2L \xrightarrow{+e^-} Cp^*Fe(CO)^{\cdot}{}_2 + L^-$$

$$2Cp^*Fe(CO)^{\cdot}{}_2 \longrightarrow [Cp^*Fe(CO)_2]_2$$

($Cp^* = \eta$-C_5H_5 or η-C_5Me_5; L = SC(S)OEt)

This is in accord with the one-electron reduction obtained in the exhaustive electrolysis and with the polarographic and IR examination [39] of the resulting solution ($[\eta$-$C_5H_5Fe(CO)_2]_2$; ν(CO) 1992, 1950 and 1784 cm^{-1}; $[\eta$-$C_5Me_5Fe(CO)_2]_2$; ν(CO) 1921, 1758 cm^{-1}). Furthermore, the potential peaks of B and B′ are identical with the cathodic and anodic peaks of the corresponding dimers (Figs. 5 and 6) (Table VII), and the peaks about +0.5 V are coincident with the oxidation peak from cyclic voltammograms of KSC(S)OEt solutions.

It has been reported [40] that in the steady-state cyclic voltammogram of $[\eta$-$C_5H_5Fe(CO)_2]_2$ in acetonitrile, cathodic and anodic peaks are observed. The process corresponds to the reduction of the iron dimer at cathodic peak (B) and the oxidation of a reaction product, presumably $[\eta$-$C_5H_5Fe(CO)_2]^-$, B′. The reduction step involves the formation of an anion radical followed by a decomposition reaction:

$$[CpFe(CO)_2]_2 + e^- \rightleftharpoons [CpFe(CO)_2]_2^{\cdot-}$$

$$[CpFe(CO)_2]_2^{\cdot-} \xrightarrow{K} CpFe(CO)_2^{\cdot} + CpFe(CO)_2^-$$

$$CpFe(CO)_2^{\cdot} + [CpFe(CO)_2]^{\cdot} \xrightarrow{\text{fast}} CpFe(CO)_2^- + [CpFe(CO)_2]_2$$

Upon going to either lower temperatures or higher sweep rates the oxidation of the anion radical regenerating $[CpFe(CO)_2]_2$ can be observed on the reverse scan. In our case this peak, B'_1, may be the consequence of a reaction which involves the initial depolarizer, presumably:

$$Cp^*Fe(CO)_2 + Cp^*Fe(CO)_2L \longrightarrow [Cp^*Fe(CO)_2]^{\cdot} + L^-$$

The cyclic voltammograms of the complex η-$C_5H_5Fe(CO)_2(\eta^1$-SC(S)OEt) (**1**) at a hanging mercury electrode (HMDE) display three cathodic and two anodic peaks in the first run and other additional cathodic peak in the second and following scan which form a reversible pair with the cathodic peak located at less negative potentials (Fig. 7) (Table VII).

The electrochemical reduction is diffusion controlled with the anodic current function independent of scan rates, ν, over the range studied. The magnitude of the slopes in the plots of *Ep versus* log ν

TABLE VII. Cyclic Voltammetric Data (V)[a] for the Complexes at 200 mV s^{-1} in THF Solution

	C glassy electrode					HMDE electrode				
	Ep_A	Ep_B	$Ep_{B'}$	$Ep_{B'_1}$	L[b]	Ep_A	Ep_B	Ep_C	$Ep_{C'}$	L[b]
η-$C_5H_5Fe(CO)_2(\eta^1$-SC(S)OEt (**1**)	−1.38	−1.78	−0.89	−1.42[c]	+0.52	−1.13	−1.25	−1.64	−1.20	−0.52/−0.45
η-$C_5Me_5Fe(CO)_2(\eta^1$-SC(S)OEt) (**2**)	−1.58	−2.09	−1.06	−1.80	+0.53	−1.42	−2.02	−2.42	−1.27	−0.54/−0.46
$[\eta$-$C_5H_5Fe(CO)_2]_2$		−1.74	−0.84					−1.74	−1.18	
$[\eta$-$C_5Me_5Fe(CO)_2]_2$		−2.10	−1.04				−2.05	−2.40	−1.27	

[a] *vs.* an SCE reference electrode. [b] $L = SC(S)OEt^-$. [c] At 50 mV s^{-1}.

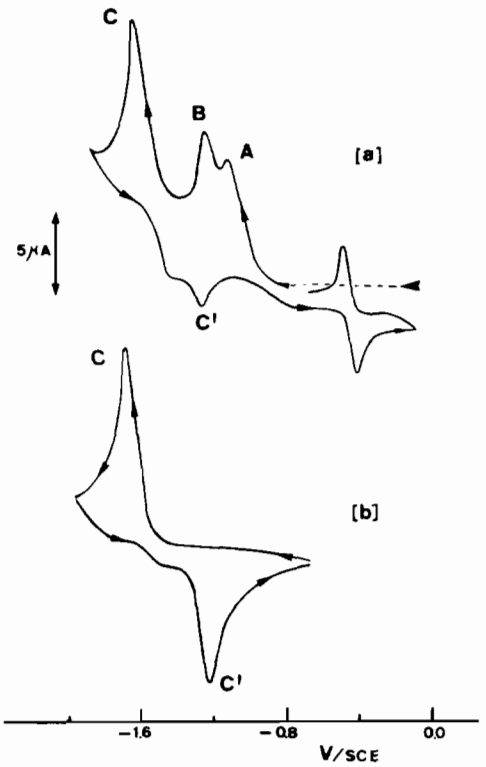

Fig. 7. Cyclic voltammogram in THF solution, containing 0.1 M Bu_4NPF_6, at a HMDE, scan rate 0.2 V s^{-1} for: (a) η-$C_5H_5Fe(CO)_2(\eta^1$-SC(S)OEt) (**1**), (b) $[\eta$-$C_5H_5Fe(CO)_2]_2$.

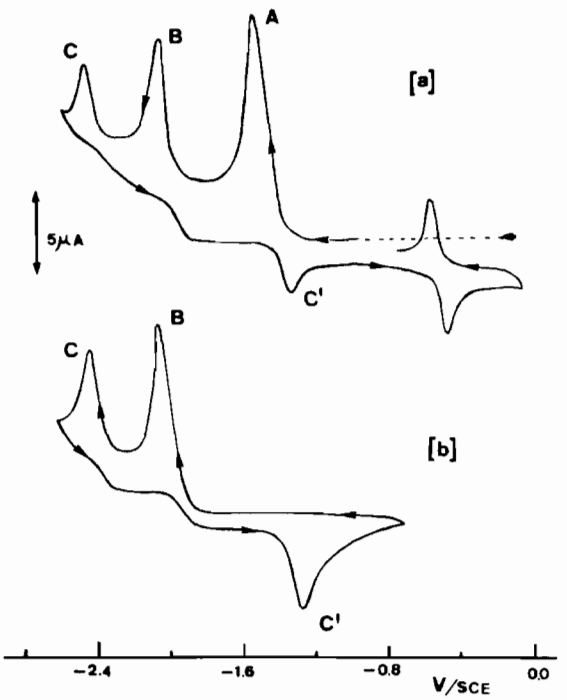

Fig. 8. Cyclic voltammogram in THF solution, 0.1 M Bu_4NPF_6, at a HMDE, scan rate 0.2 V s^{-1} for: (a) η-$C_5Me_5Fe(CO)_2(\eta^1$-SC(S)OEt) (**2**). (b) $[\eta$-$C_5Me_5Fe(CO)_2]_2$.

indicates the irreversibility of the electron transfers corresponding to peaks A and B.

The exhaustive electrolysis at a mercury pool cathode shows that for complete reduction at potentials close to *Ep* of the first reduction peak, one electron per particle of depolarizer is consumed. The polarographic and spectrophotometric examination of the reduced solution indicates that the product formed is $[\eta$-$C_5H_5Fe(CO)_2]_2Hg$ (ν(CO): 1980, 1950, 1921 cm^{-1}; λ = 388 nm [41, 42]).

From these experiments it follows that the mechanism of the first reduction step can be described by the scheme:

$$\eta\text{-}C_5H_5Fe(CO)_2L \xrightarrow{+e^-} [\eta\text{-}C_5H_5Fe(CO)_2]^{\cdot}_{ad} + L^-$$

$$\downarrow \text{Hg}$$

$$[\eta\text{-}C_5H_5Fe(CO)_2]_2Hg$$

L = SC(S)OEt

Analogous results have been reported by Miholova and Vlček [43] for the electrochemical reduction of η-$C_5H_5Fe(CO)_2X$ (X = Cl, Br, I, $SiCl_3$, $GeCl_3$). The radical forms a mercury compound in a chemical surface reaction; this compound is electrochemically reduced at about −1.2 V, peak B, to form the anion $[\eta$-$C_5H_5Fe(CO)_2]^-$ [39, 41], which can give the reactions*:

$$[CpFe(CO)_2]_2Hg + CpFe(CO)_2^- \longrightarrow [CpFe(CO)_2]_3Hg^-$$

and

$$[CpFe(CO)_2L] + CpFe(CO)_2^- \longrightarrow [CpFe(CO)_2]_2 + L^-$$

Cp = η-C_5H_5; L = SC(S)OEt

The cyclic voltammogram of the dimer $[\eta$-$C_5H_5Fe(CO)_2]_2$ shows a pair of cathodic and anodic peaks. The potential peaks of C and C′ are near to the corresponding peaks of the dimer. However, the peak C can be adscribed in cyclic voltammetry to the reduction to $[\eta$-$C_5H_5Fe(CO)_2]^-$ of either $[CpFe(CO)_2]_2$ and $[CpFe(CO)_2]_3Hg^-$ because these compounds have reduction potentials very close. Potentiostatic coulometry indicates the consumption of two electrons per molecule of initial depolarizer for the process that takes place at potentials 100 mV more negative than Ep_C, being identified η-$C_5H_5Fe(CO)_2^-$ (ν(CO): 1868, 1792 and 1772 cm^{-1}) as the product of the electrode reaction.

*There is no interaction between $CpFe(CO)_2L$ and $[CpFe(CO)_2]_2Hg$ as has been shown in ref. 43.

On the other hand the peak C′ corresponds to the process [41]:

$$[\eta\text{-}C_5H_5Fe(CO)_2]^- + \tfrac{1}{2}Hg \xrightarrow{-e^-} \tfrac{1}{2}[CpFe(CO)_2]_2Hg$$

The first peak, A, in the cyclic voltammograms of η-$C_5Me_5Fe(CO)_2(\eta^1$-SC(S)OEt) (2) displays the same electrochemical characteristics as for the cyclopentadienyl analogue (1). However, the potential peak of B and C are very close (Table VII, Fig. 8) to the two cathodic peaks shown by the respective dimer $[\eta\text{-}C_5Me_5Fe(CO)_2]_2$. This suggest that the reduction product of 2 in the first step could be the dimer, in the time-scale of cyclic voltammetry, because attempts to detect it after exhaustive electrolysis at a mercury pool are unsuccessful.

When the complete electroreduction is carried out at potentials 100 mV after Ep_B and Ep_C 1.4 and 2 Faradays/mol are required respectively. Thus, peak C can be identified as being due to the reduction of a mercury complex, $[\eta\text{-}C_5Me_5Fe(CO)_2]_{2+x}Hg^{x-}$, this compound being stabilized by an excess of anion $[\eta\text{-}C_5Me_5Fe(CO)_2]^-$; however this extreme needs further investigation.

The releasing of the xanthate ligand by all compounds is proved by the CVs of the KSC(S)OEt solutions; the potential peaks observed are identical with the respective anodic and cathodic peaks of the reversible system that appears at more positive potentials [44].

The different electrochemical behaviour of pentamethylcyclopentadienyl compounds may be related to the difference between the peralkylcyclopentadienylmetal complexes compared with the corresponding unsubstituted cyclopentadienyl compound with respect to reactivity in carbonyl substitution reactions [11] and in catalytic activity [9, 10].

The more negative reduction potentials observed for the η-$C_5Me_5Fe(CO)_2(\eta^1$-SC(S)OEt) compound are due to the greater electron donor ability of the pentamethylcyclopentadienyl ligand, which leads to a higher electron density around the metal atom.

Supplementary Material

Lists of hydrogen atom positions, thermal parameters and observed/calculated structure factors are available from the authors on request.

Acknowledgements

The authors thank CAICYT (Comisión Asesora de Investigación Científica y Técnica, project 415/84, Spain) for financial support. We also thank BASF AG (Ludwigshafen, F.R.G.) for a generous gift of $Fe(CO)_5$ and Prof. V. Fernández for helpful discussions.

References

1 G. Winter, *Rev. Inorg. Chem., 2*, 253 (1980).
2 D. Concouvanis, *Prog. Inorg. Chem., 22*, 301 (1979).
3 R. Eisenberg, *Prog. Inorg. Chem., 12*, 295 (1970).
4 D. Concouvanis, *Prog. Inorg. Chem., 11*, 233 (1970).
5 J. Takács and L. Markó, *Transition Met. Chem., 9*, 10 (1984).
6 O. P. Pandey, S. K. Sengupta and S. C. Tripathy, *Polyhedron, 3*, 695 (1984).
7 R. S. P. Coutts, P. C. Wailes and J. V. Kingston, *Aust. J. Chem., 23*, 469 (1970).
8 C. Tsipis, G. E. Manoussakis, D. P. Kessissoglou, J. C. Huffman, L. N. Lewis, M. A. Adams and K. G. Caulton, *Inorg. Chem., 19*, 1458 (1980).
9 E. Cesarotti, A. Fusi, R. Ugo and G. M. Zarderighi, *J. Mol. Catal., 4*, 205 (1978).
10 A. Fusi, E. Cesarotti and R. Ugo, *J. Mol. Catal., 10*, 213 (1981).
11 K. Tabatabain and C. White, *Inorg. Chem., 20*, 2020 (1981).
12 H. Adams, N. A. Bailey and C. White, *Inorg. Chem., 22*, 1155 (1983).
13 M. Morán, I. Cuadrado, C. Muñoz-Reja, J. R. Masaguer and J. Losada, *J. Chem. Soc., Dalton Trans.*, in press.
14 D. A. Ramsay, *J. Am. Chem. Soc., 74*, 73 (1952).
15 P. T. Beurskens, W. P. Bosman, H. H. Doesburs, R. O. Gould, Th. E. M. van den Hark, P. A. J. Prick, J. H. Noordik, G. Beurskens, V. Parthasarathi, H. J. Bruins Slot, R. C. Haltiwanser and J. M. M. Smits, 'Dirdif System', Crystallography Laboratory, Toernooiveld, Nijmegen, The Netherlands, 1984.
16 N. Walker and D. Stuart, *Acta Crystallogr., Sect. A, 39*, 158 (1983).
17 J. M. Stewart, P. A. Machin, C. W. Dickinson, H. L. Ammon, H. Heck and H. Flack, 'X-ray System', *Technical Report TR-166*, Computer Science Center, University of Maryland, U.S.A., 1976.
18 'International Tables for X-ray Crystallography', Vol. IV, Kynoch Press, Birmingham, U.K., 1974.
19 D. A. Stephens and J. M. Williams, *Inorg. Synth., 24*, 141 (1986).
20 C. K. Johnson, 'ORTP', *Report ORNL-3794*, Oak Ridge National Laboratory, Tenn., U.S.A., 1965.
21 M. J. Barrow and G. A. Sim, *J. Chem. Soc., Dalton Trans.*, 291 (1975).
22 M. R. Churchill and S. W. V. Nichang, *J. Am. Chem. Soc., 95*, 593 (1973).
23 H. Brunner, J. Wachter, E. Guggolz and M. L. Ziegler, *Organometallics, 1*, 1107 (1982).
24 J. T. Malito, R. Shaki and J. L. Atwood, *J. Chem. Soc., Dalton Trans.*, 1253 (1980).
25 N. W. Alcock, G. E. Toogood and M. G. H. Wallbridge, *Acta Crystallogr., Sect. C, 40*, 598 (1984).
26 D. P. Freyberg, J. L. Robbins, K. N. Raymond and J. C. Smart, *J. Am. Chem. Soc., 101*, 892 (1979).
27 R. G. Teller and J. M. Williams, *Inorg. Chem., 19*, 2770 (1980).
28 D. J. Sikosa, M. D. Rausch, R. D. Rogers and J. L. Atwood, *J. Am. Chem. Soc., 103*, 1265 (1981).
29 F. A. Cotton and C. S. Kraihanzel, *J. Am. Chem. Soc., 84*, 4432 (1962).
30 D. J. Darensbourg, *Inorg. Chem., 11*, 1606 (1972).
31 J. Dalton, I. Paul and F. G. A. Stone, *J. Chem. Soc. A*, 2744 (1969).
32 R. B. King, *Inorg. Chim. Acta, 2*, 454 (1968).
33 M. Morán and I. Cuadrado, *J. Organomet. Chem., 295*, 353 (1985).
34 W. P. Anderson and T. L. Brown, *J. Organomet. Chem., 32*, 343 (1971).

35 D. J. Darensbourg and T. L. Brown, *Inorg. Chem., 7*, 959 (1968).
36 D. J. Darensbourg, *Inorg. Chim. Acta, 4*, 597 (1970).
37 D. T. Clark and D. B. Adams, *J. Chem. Soc., Chem. Commun.*, 740 (1971).
38 R. J. Klinger and J. K. Kochi, *J. Am. Chem. Soc., 102*, 4790 (1980).
39 M. Morán, I. Cuadrado and J. Losada, *J. Organomet. Chem., 320*, 317 (1987).
40 S. G. Davies, S. J. Simpson and V. D. Parker, *J. Chem. Soc., Chem. Commun.*, 352 (1984).
41 D. Miholova and A. A. Vleck, *Inorg. Chim. Acta, 41*, 119 (1980).
42 J. M. Burlitch and A. Ferrari, *Inorg. Chem., 9*, 563 (1970).
43 D. Miholova and A. A. Vleck, *Inorg. Chim. Acta, 43*, 43 (1980).
44 A. M. Bond, A. T. Casey and J. R. Thackeray, *J. Electroanal. Chem., 48*, 71 (1973).